BIOCHEMISTRY
including biophysical chemistry & molecular biology

Article

pubs.acs.org/biochemistry

Rational Design of α-Helix-Stabilized Exendin-4 Analogues

Petra Rovó,[†] Viktor Farkas,[‡] Pál Stráner,[‡] Mária Szabó,[‡] Ágnes Jermendy,[§] Orsolya Hegyi,[∥] Gábor K. Tóth,[∥] and András Perczel*[,†,‡]

[†]Laboratory of Structural Chemistry and Biology, Institute of Chemistry, Eötvös Loránd University, Budapest, Hungary

[‡]MTA-ELTE Protein Modelling Research Group, Budapest, Hungary

[§]1st Department of Paediatrics, Semmelweis University, Budapest, Hungary

[∥]Department of Medical Chemistry, Faculty of General Medicine, University of Szeged, Szeged, Hungary

Supporting Information

ABSTRACT: Exendin-4 (Ex4) is a potent glucagon-like peptide-1 receptor agonist, a drug regulating the plasma glucose level of patients suffering from type 2 diabetes. The molecule's poor solubility and its readiness to form aggregates increase the likelihood of unwanted side effects. Therefore, we designed Ex4 analogues with improved structural characteristics and better water solubility. Rational design was started from the parent 20-amino acid, well-folded Trp cage (TC) miniprotein and involved the step-by-step N-terminal elongation of the TC head, resulting in the 39-amino acid Ex4 analogue, E19. Helical propensity coupled to tertiary structure compactness was monitored and quantitatively analyzed by electronic circular dichroism and nuclear magnetic resonance (NMR) spectroscopy for the 14 peptides of different lengths. Both ^{15}N relaxation- and diffusion-ordered NMR measurements were established to investigate the inherent mobility and self-association propensity of Ex4 and E19. Our designed E19 molecule has the same tertiary structure as Ex4 but is more helical than Ex4 under all studied conditions; it is less prone to oligomerization and has preserved biological activity. These conditions make E19 a perfect lead compound for further drug discovery. We believe that this structural study improves our understanding of the relationship between local molecular features and global physicochemical properties such as water solubility and could help in the development of more potent Ex4 analogues with improved pharmacokinetic properties.

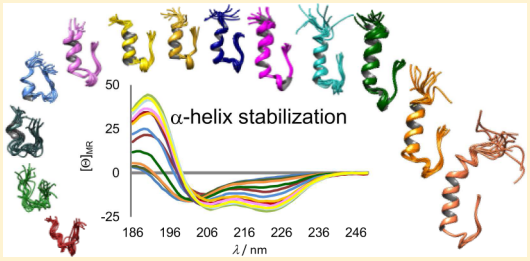

Exendin-4 (Ex4), a 39-amino acid polypeptide secreted by the lizard *Heloderma suspectrum*, shares common bioactivity with the human incretin glucagon-like peptide-1 (GLP-1).[1] Both Ex4 and GLP-1 bind to the GLP-1 receptor (GLP-1R) and potentiate the secretion of insulin from pancreatic β-cells.[2,3] Because of its high binding affinity and extended *in vivo* half-life, Ex4 and its analogues have been a focus for the treatment of type 2 diabetes.[4−7]

The structure of Ex4 has been determined by both ^{1}H NMR spectroscopy and X-ray crystallography.[8,9] Because the solubility of Ex4 in H_2O is limited, its NMR spectra have been acquired in a 30% trifluoroethanol (TFE)/70% H_2O mixture[8] while the X-ray structure of a truncated Ex4 [Ex4(9−39)] has been determined in a GLP-1R-bound state.[9] Ex4 displays significant helicity from residue 7 to 28 with greater fraying at the N-terminus and is stabilized by a Trp cage (TC) tertiary fold at the C-terminal part of the helix. The comparison of the NMR and X-ray structures reveals that the TFE/H_2O medium can mimic the receptor-bound state as the two types of Ex4 conformers superimpose well.

The N-terminal segment of Ex4 is 82% homologous with human GLP-1(7−36); conserved residues include His[1], Glu[3], Thr[5], and Phe[6], all of which are crucial for receptor activation (Figure 1).[10−12] The affinity of Ex4 for the GLP-1 receptor's N-terminal domain (nGLP-1R) is governed by the central helical part of the molecule.[13] Both hydrophobic and hydrophilic side chains are involved in the binding as revealed by the crystal structure of the complex [Protein Data Bank (PDB) entry 3C5T].[9] The binding surface of Ex4 consists of Glu[15], Val[19], Arg[20], Phe[22], Ile[23], Leu[26], Lys[27], and Ser[32], whereas that of nGLP-1R involves Leu[32], Thr[35], Val[36], Trp[39], Tyr[69], Tyr[88], Leu[89], Pro[90], Trp[91], Leu[123], Glu[127], and Glu[128].[9]

On the basis of recent structure−activity studies, it is known that all peptidic ligands targeting class B G-protein-coupled receptors (GPCRs) bind in a predominantly α-helical manner, and for most ligands, the α-helix forms upon binding of the extracellular N-terminal domain of the GPCR.[15] These ligands, including glucagon,[16] GLP-1,[8,17] GLP-2,[18] Ex4,[8] glucose-dependent insulinotropic polypeptide (GIP),[19] pituitary adenylate cyclase activating polypeptide (PACAP),[20] and corticotropin-releasing factor (CRF),[21] show moderately ordered structure in aqueous solution but adopt a continuous or kinked α-helix in the presence of organic solvents (e.g., in a TFE/water mixed solvent) or in protein crystals. The major structural difference between Ex4 and GLP-1 is the continuity of the α-helix: Ex4 forms a single amphipathic α-helix both in the TFE/

Received: January 9, 2014
Revised: May 13, 2014
Published: May 14, 2014

   dx.doi.org/10.1021/bi500033c | *Biochemistry* 2014, 53, 3540−3552

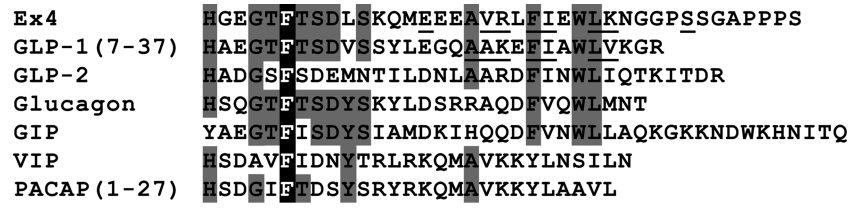

Figure 1. Sequence alignment of class B GPCR ligands. Amino acids on a black background represent fully conserved residues, and amino acids on a gray background represent four to six identical residues among the seven listed class B GPCR ligands. Residues that interact with nGLP-1R are underlined.[9,14]

water mixed solvent and in the receptor-bound state, while GLP-1 is composed of two adjacent subhelices joined by the flexible Gly[22].

Binding studies demonstrated that the isolated N-terminal extracellular domain of GLP-1R has a low affinity for endogenous GLP-1 but a high affinity for Ex4.[22] The superior affinity of Ex4 stems from the more favorable alignment of the oppositely charged hydrophilic residues at the receptor binding site and from the enhanced α-helical propensity of Ex4 in solution.[9,23] Previous studies found a positive correlation between the α-helical propensity of the ligand and its affinity for nGLP-1R.[23] It was proposed that the C-terminal extension of Ex4, which is absent in GLP-1, has only a minor role in mediating receptor binding; thus, this segment cannot be the source of the high binding affinity. However, we suppose that the latter nine-residue C-cap, PSSGAPPPS, has a definite role in fine-tuning the structure of the Ex4 α-helix and in preforming the receptor-bound conformation in solution. We propose that the extension described above makes the TC fold an ideal C-cap of a more stable α-helix.[12,22,24,25]

Studies of the aggregation ability of different class B GPCR ligands (e.g., calcitonin,[26,27] glucagon,[28] or GLP-1[29]) determined that these peptides can form cytotoxic amyloid aggregates that could be a drawback for their usage as protein drugs. In liquid formulations, these peptides tend to self-associate and assemble into transient helix bundles[25] and over time form aggregates.[30] Of particular concern is the fact that the peptide aggregates increase the risk of immunogenicity.[31] Therefore, chemical modifications (e.g., site specific mutations or side-chain conjugation) need to be considered to obtain therapeutic candidates that are more soluble, more stable, and thus safer than the existing drug.

Following these guidelines, we designed Ex4 analogues, including a potential GLP-1R agonist (E19) and several antagonists (E0–E11), using the optimized TC miniprotein as a starting sequence.[32,33] The procedure incorporated the replacement of specific residues into the Ex4 sequence to increase the peptide's helicity and meanwhile reduce its ability to self-assemble. As a result of this design, E19 is now more soluble in pure water, less prone to aggregation, and under all conditions more helical than Ex4. Moreover, it shows an insulin secreting activity comparable to that of Ex4.

EXPERIMENTAL PROCEDURES

Ex4 numbering is used throughout this paper. The numbers in the names of the Ex4/TC analogues indicate the length of the N-terminal elongation with respect to the reference TC molecule; E0 has no N-terminal elongation but an N-terminal Asn to Arg mutation, while E19 has 19 extra N-terminal residues, all taken from Ex4. Thus, the lengths of E19 and Ex4 are the same.

Peptide Synthesis and Purification. Peptides E0–E10 were prepared by standard solid-phase peptide synthesis protocols. MBHA resin was used as solid support, and the following side-chain protecting groups were used: Boc-Ser(Bzl), Boc-Arg(Tos), Boc-Glu(OcHex), Boc-Tyr(2BrZ), and Boc-Lys(2ClZ). Couplings were performed with DCC and HOBt. Amino acid incorporation was monitored by the quantitative ninhydrin test. The completed peptide resins were treated with a liquid HF/dimethyl sulfide/*p*-cresol/*p*-thiocresol mixture [86:6:4:2 (v/v)] at 0 °C for 45 min. HF was removed, and the resulting free peptides were solubilized in 10% aqueous acetic acid, filtered, and lyophilized. The crude peptides were purified by reverse-phase high-performance liquid chromatography (HPLC) on a Phenomenex Jupiter C-18 column (21.2 mm × 250 mm), using a water/acetonitrile gradient (solvent system of 0.1% TFA in water and 0.1% TFA and 80% acetonitrile in water, gradient from 0 to 40% B over 80 min, flow rate of 3 mL/min, and detection at 220 nm). Collected fractions were lyophilized, and their identities were confirmed by a Finnigan TSQ 7000 tandem quadrupole mass spectrometer equipped with an electrospray ion source.

Peptide Expression and Purification. Peptides E5, E11, E19, and Ex4 were produced by recombinant methods using published protocols.[34] Briefly, the cDNAs of the peptides were ligated into a SacII and BamHI site of the pUBK2 vector. The plasmid encoding H10-Ub-Peptide was transformed into *Escherichia coli* strain BL21(DE3). Transformed cells were grown in LB medium containing 0.1 mg/mL kanamycin and incubated while being shaken at 37 °C. Cells were induced at an OD_{600} of 0.6–0.8 by addition of IPTG (isopropyl β-D-1-thiogalactopyranoside) to a final concentration of 1 mM. After incubation for 3 h at 37 °C, cells were harvested, resuspended in lysis buffer (300 mM NaCl, 50 mM NaH_2PO_4, and 3 mM NaN_3), and lysed by sonication. The pellet was removed by centrifugation, and the target protein was dissolved in the supernatant. All proteins were purified using a 5 mL nickel-nitrilotriacetic acid (Ni-NTA) chromatography column. The column was equilibrated and washed with lysis buffer, and then the fusion protein was eluted with the same lysis buffer containing 250 mM imidazole. The eluted fractions were dialyzed overnight into lysis buffer, and then the fusion proteins were digested with His-tagged yeast ubiquitin hydrolase (YUH) for 3–4 h. The digestion efficiency was followed by sodium dodecyl sulfate–polyacrylamide gel electrophoresis. The ubiquitin and YUH were separated from the peptides by Ni affinity chromatography. Peptides were further purified by reverse-phase HPLC on a C-18 column using a water/acetonitrile gradient (eluent A being 0.1% TFA in water and eluent B being 0.08% TFA and 80% acetonitrile in water). Collected fractions were lyophilized, and their identities were confirmed by a Perkin-Elmer Sciex API2000 mass spectrometer equipped with an electrospray ion source.

Electronic Circular Dichroism Spectroscopy. Far- and near-UV ECD spectra were recorded on a Jasco J810

dx.doi.org/10.1021/bi500033c | *Biochemistry* 2014, 53, 3540–3552

spectrophotometer using cuvettes with a path length of 1.0 or 10 mm with protein concentrations of 35−150 μM. Typical spectral accumulation parameters were a scan rate of 50 nm/min with a 1 nm bandwidth and a 0.2 nm step resolution over wavelength ranges of 185−260 nm (far-UV) and 250−325 nm (near-UV) with four scans averaged for each spectrum. The temperature at the cell was controlled by a Peltier-type heating system. The solvent reference spectra were used as baselines that were automatically subtracted from the peptide spectra. The raw ellipticity data were converted into mean residue molar ellipticity units ($[\Theta]_{MR}$, degrees square centimeters per decimole).

Nuclear Magnetic Resonance Spectroscopy. NMR spectra were recorded on a Bruker DRX 500 or 700 MHz spectrometer or a Varian VXR 800 MHz spectrometer using ∼1 mM peptide samples between pH 6.5 and 7.1, with 10% D_2O and 0.1 mM NaN_3. DSS was used as the internal proton reference standard set to 0.0 ppm for all conditions. Data sets were processed using TopSpin (Bruker Biospin, Inc.). Proton NMR chemical shift assignments were achieved using standard procedures that required the recording of ^{1}H−^{1}H TOCSY and ^{1}H−^{1}H NOESY spectra and were completed using Sparky.[35] TOCSY measurements were taken with spin locks of 65−80 ms, and mixing times of 100−300 ms were used for the NOESY spectra. The chemical shift deviations were calculated using the reference random coil shifts determined by Bundi et al.[36] The number of overlapping peaks increased with the length of the polypeptide chains; therefore, spectra of E9−E11, E19, and Ex4 were acquired on higher-field instruments (700 and 800 MHz). For Ex4 and E19, heteronuclear three-dimensional (3D) HSQC-TOCSY and HSQC-NOESY spectra were also used to facilitate the complete resonance assignment. The NMR spectra of E0−E11 were recorded at 5 °C, those of E11 at both 5 and 27 °C, and those of E19 and Ex4 at 27 °C. The NMR structures were determined following standard procedures. The NOE cross-peak intensities were converted into distance restraints and calibrated using the covalently fixed distances of the indole side-chain protons. Structure calculations were performed with CNS Solve version 1.1.[37] All structural figures in this report were prepared using Chimera.[38]

Diffusion-ordered spectroscopy (DOSY) experiments were recorded for ∼0.5 mM peptides in a 10% D_2O/90% H_2O or 30% TFE-d_2/70% H_2O mixture at 5, 16, and 27 °C. The strength of the B_0 field was calibrated using the residual HDO signal of 100% D_2O. The diffusion time (Δ) was varied between 100 and 220 ms, while the gradient pulse duration (δ) was set to 4 ms in all experiments. The pulse gradient was incremented from 2 to 95% of the maximal gradient strength in a linear manner in 32 steps. Data analyses were performed using the T_1/T_2 relaxation routine of Topspin version 3.2. Diffusion coefficients were obtained by fitting the peak intensities in the aliphatic and in the methyl region to a single-exponential decay: $I = I_0 \exp[-\gamma^2 g^2 D\delta^2(\Delta - \delta/3)]$, where I is the peak intensity, γ is the gyromagnetic ratio, and g, δ, and Δ are the amplitude, duration, and separation of the gradient pulses, respectively. The obtained diffusion coefficients were converted to standard conditions (20 °C, water)[39] using the viscosity of water (1.002×10^{-3} N s m^{-2}) and a 30% TFE/70% H_2O solution (1.606×10^{-3} N s m^{-2}).[39] From the diffusion coefficient, apparent molecular masses (M_w) were derived using eq 4 of ref 39, assuming a prolate ellipsoid with an axial ratio (p) of 0.33, a partial specific volume (v_2) of 0.72×10^{-3} m^3 kg^{-1}, and a hydration number (δ_1) of 0.4.

Backbone ^{15}N longitudinal (R_1) and transverse (R_2) relaxation rates and the heteronuclear ^{1}H−^{15}N cross-relaxation rate constant (NOE) of TC, E5, and E11 were measured at 500 MHz and 27 °C, while that of E19 was measured at 27 °C at 500 and 700 MHz using published pulse schemes.[40,41] Relaxation rates were recorded at eight different relaxation delays between 10 and 1100 ms for R_1 and 15 and 400 ms for R_2. ^{1}H−^{15}N NOE were obtained from two spectra recorded with or without proton saturation. R_1 and R_2 rates were estimated by fitting the cross-peak intensities with a two-parameter exponential decay: $I(T) = I_0 \exp(TR)$, where $I(T)$ is the peak intensity, T is the relaxation delay, I_0 is the intensity at zero time, and R is the relaxation rate. ^{1}H−^{15}N NOE values were determined from the I_{sat}/I_{ref} ratio, where I_{sat} and I_{ref} are the peak intensities with and without proton presaturation, respectively.[42] All relaxation parameters are given in the Supporting Information.

Reduced spectral density mapping was performed using published methods with an amide bond length of 1.02 Å and a chemical shift anisotropy of the ^{15}N nucleus of 160 ppm.[40,43−45]

Cell Culture. Rat β-cell line INS-1E was a kind gift of P. Maechler (University of Geneva, Geneva, Switzerland). INS-1E cells were cultured in a humidified atmosphere containing 5% CO_2 in complete medium composed of RPMI 1640 supplemented with 10% heat-inactivated fetal bovine serum, 1 mM sodium pyruvate, 50 μM 2-mercaptoethanol, 2 mM glutamine, 10 mM HEPES, 100 units/mL penicillin, 100 μg/mL streptomycin, and 250 ng/mL Amphotericin-B.[46] Cells were between passages 100 and 120 at the time of the experiments.

Insulin Secretion. The secretory response of INS-1E cells was tested in response to Ex4, E19, and E10. Simulated insulin secretion experiments followed the protocol of Merglen et al.[46] In brief, cells were maintained for 2 h in glucose-free culture medium before the experiments. The cells were then washed twice and preincubated for 30 min at 37 °C in Krebs-Ringer bicarbonate HEPES buffer (KRBH) that consisted of 2.5 mM glucose, 135 mM NaCl, 3.6 mM KCl, 5 mM $NaHCO_3$, 0.5 mM NaH_2PO_4, 0.5 mM $MgCl_2$, 1.5 mM $CaCl_2$, 0.1% bovine serum albumin, and 10 mM HEPES (pH 7.4). The cells were washed once with glucose-free KRBH and then incubated for 30 min in KRBH containing 15 mM glucose and the respective GLP-1 receptor agonist at 20 nM. After the 30 min incubation, supernatants were collected for insulin secretion analysis (Ex4, E19, and E10). Insulin concentrations of the collected supernatants were determined by the rat insulin enzyme-linked immunosorbent assay (Alpco Diagnostics, Salem, NH). In the absence of peptide (15 mM glucose), the measured insulin concentration of the collected supernatant served as a baseline. The stimulated insulin release is expressed as the fold change in insulin concentration in response to various GLP-1 receptor stimuli (Ex4, E19, and E10) as compared to basal stimulatory conditions (15 mM glucose). Values are given as means ± the standard error of mean, and n values refer to the number of experiments. The significance of the differences was assessed by a one-tailed t test.

RESULTS

The parent molecule of our study was the 20-residue Trp cage miniprotein (NLYIQ WLKEG GPSSG RPPPS), originally derived from Ex4 by truncating its first 19 N-terminal residues and by modifying the remaining sequence at five structurally essential positions.[32,33,47] During the design process, we applied this structurally optimized TC motif now as part of Ex4, to enhance the overall helicity and water solubility of the nGLP-1R agonist. Rational protein design involved the insertion of a

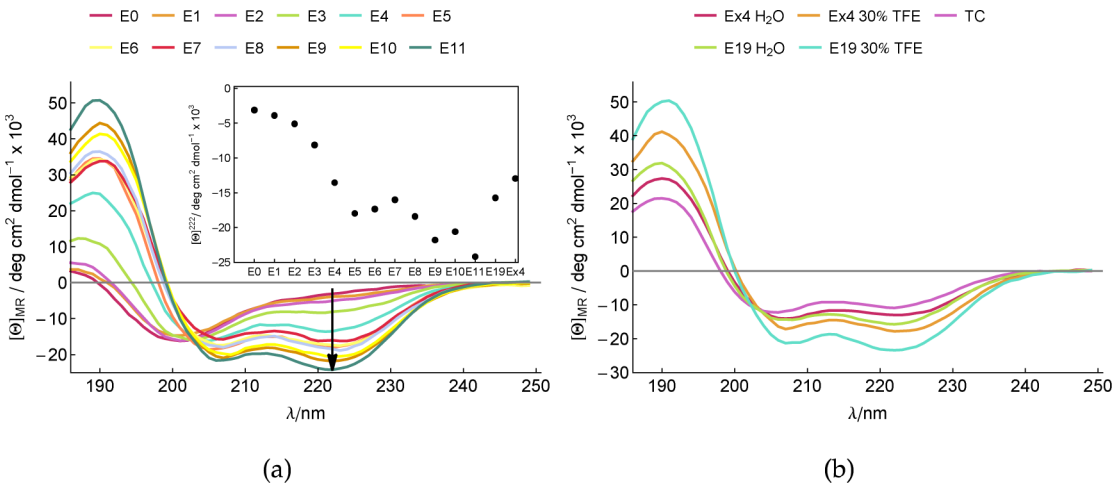

Figure 2. Far-UV ECD spectra of (a) E0−E11 (measured in H_2O) and (b) TC, E19, and Ex4 (measured in H_2O or 30% TFE) at 5 °C. The inset in panel a displays the molar ellipticity values at 222 nm for each peptide (E0−E11, E19, and Ex4, all in H_2O).

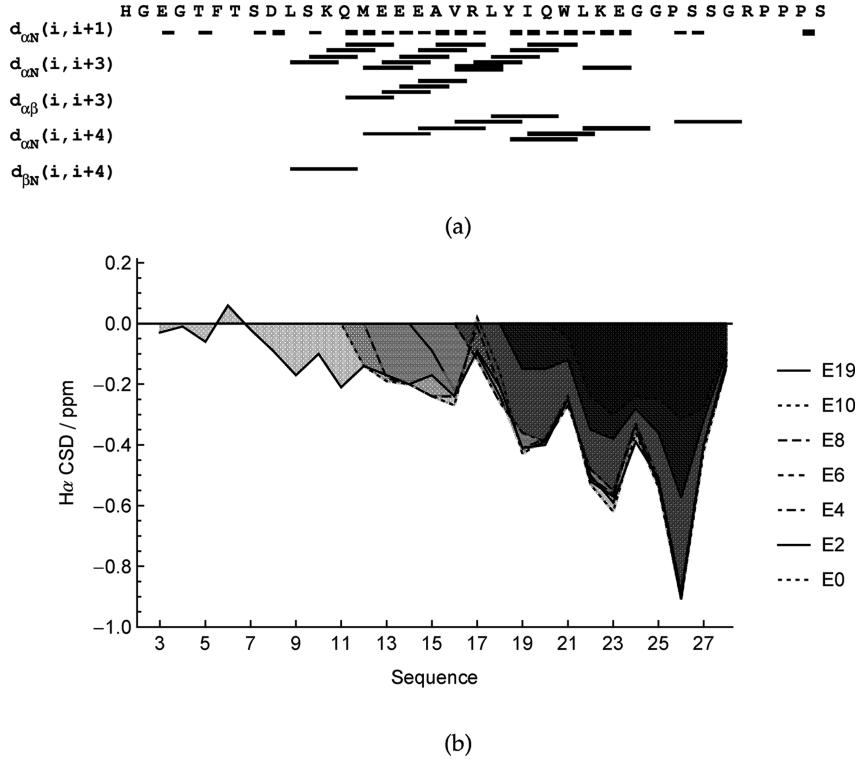

Figure 3. (a) NOE connectivity chart of E19 displaying short- and medium-range NOEs. The thickness of the lines is scaled with the distance restraints. (b) Hα chemical shift deviations from their random coil values of E19, E10, E8, E6, E4, E2, and E0 in the E^3−E^{28} segment. The corresponding Hα CSD plot of E11, E9, E7, E5, E3, and E1 is displayed in Figure S2 of the Supporting Information.

Glu^{28}−Arg^{35} salt bridge[a] and the replacement of Phe^{22} and Glu^{24} with Tyr^{22} and Gln^{24}, respectively.

The N28E and A35R modifications of the Ex4 sequence have multiple benefits. (i) The salt bridge stabilizes the overall structure, thereby increasing the folded population and improving the helicity.[32,33,47,48] (ii) The side chains of the salt bridge-forming residues cover the indole ring of Trp^{25}; thus, they reduce the water-accessible hydrophobic surface area. (iii) The charged side chains of Glu^{28} and Arg^{35} improve the peptide's water solubility. The F22Y modification improved the π−π stacking interaction with Trp^{25} and increased the hydrophilicity of the peptide.[32] This modification also allowed the monitoring of the compactness of the hydrophobic core (Trp → Tyr interaction) with near-UV ECD measurements. Although Phe^{22} is a highly conserved residue that directly interacts with the receptor, we surmise that the phenolic OH will not undermine the peptide's affinity for nGLP-1R because other class B GPCR ligands (e.g., VIP and PACAP) have a Tyr residue at this position (Figure 1).[49] The E24Q mutation was incorporated to avoid an unfavorable electrostatic interaction between Gln^{24} and Glu^{28} in the α-helix.[32]

In our study, we first analyze the ECD and NMR spectra of Ex4 and 14 TC elongated variants to assess the structural consequences of the introduced sequence modifications. Next, we evaluate the structural changes as a function of backbone mobility via ^{15}N relaxation measurements. Subsequently, we

dx.doi.org/10.1021/bi500033c | *Biochemistry* 2014, 53, 3540−3552

present the results of the diffusion-ordered (DOSY) NMR measurements and compare the self-association property and thus the water solubility of Ex4 and E19. Finally, we analyze the preliminary data regarding the *in vivo* insulin secreting ability of Ex4, E19, and E10 peptides.

E19 Is More Helical Than Ex4. Panels a and b of Figure 2 show the far-UV ECD spectra of all the investigated polypeptides. The Trp cage elongated variants (E0−E11) were measured at 5 °C in pure H_2O, while Ex4 and E19 were measured in both H_2O and a 30% TFE solution.

The comprehensive ECD spectral analysis revealed unexpectedly large structural changes as a function of the length of the polypeptide chain (E0−E19). The ECD spectra of Ex4, TC, and all the elongated variants from E4 to E19 display a C-type ECD curve with a positive maximum at around 190 nm and two minima at 208 and 222 nm. This characteristic ECD spectrum is often associated with α- and 3_{10}-helices as well as with repeated type I (or III) β-turns. On the other hand, the ECD spectra of E0−E3 indicate a decreased C-type and an increased U-type ECD curve propensity. The U-type curve indicates a structural ensemble of elevated internal dynamics. The ECD studies suggest that the apparent change in the helical propensities among different peptides is more the consequence of the shift between conformational populations (folded ⇌ unfolded) than the change of the structure types in the dynamic ensemble. Thus, the more intense the C-type ECD curve, the larger the peptide's folded fraction.

With the extension of E0 (resulting in E1, E2, etc.), the folded fraction gradually increases; however, the latter increase is not monotonic. Three constructs, namely, E5, E9, and E11, seem to be more helical than their N-terminal elongated partners, E6, E10, and E19, respectively (see the inset of Figure 2a). While E11 is the most helical construct among all 15 studied peptides ($[\Theta]^{191} = 49.5 \times 10^3$ deg cm^2 dmol^{-1}, $[\Theta]^{222} = -24.2 \times 10^3$ deg cm^2 dmol^{-1}, and $[\Theta]^{208} = -21.3 \times 10^3$ deg cm^2 dmol^{-1}), E19 presents a helicity similar to that of E7. E19 is less helical (or apparently less stable) than E11 because of the elevated internal mobility of the first eight N-terminal residues that were added in one step to E11 to make E19. Note that the latter eight residues must be unstructured to successfully activate the GLP-1 receptor, and thus, they will decrease the overall helicity of any agonist.[50]

Because Ex4 shows a modest level of aggregation in aqueous solution,[8] we also measured its ECD curve in a 30% TFE solution and compared it to that of E19 (Figure 2b). Clearly, E19 has superior helicity in the presence and absence of the added fluoro alcohol medium; the relative increase in helical content is 21% in H_2O and 31% in 30% TFE (measured as $[\Theta]^{222}_{E19}/[\Theta]^{222}_{Ex4} - 1$ and expressed in percent). The ECD study implies that the optimized TC motif can indeed be used to stabilize the overall fold and increase the α-helical propensity of Ex4-related peptides.

The Optimized TC Motif Stabilizes the α-Helix of Ex4. The results of the ECD spectral analysis were supplemented with homonuclear NMR measurements; similar stability differences were observed throughout the studied sequences now obtained and analyzed at the atomic level of detail.

Figure 3 and Figures S2 and S3 of the Supporting Information display the Hα chemical shift deviation (CSD) plots of the studied peptides together with the NOE connectivity chart of E19 (all other NOE charts are displayed in the Supporting Information). Generally, the negative Hα CSDs and the dense *i*,*i* + 3 and *i*,*i* + 4 NOE network indicate α-helical secondary structure for all peptides for almost all residues in the D^9−E^{28} segment. However, there are three Hα protons (E^{17}, L^{21}, and Q^{24}) with remarkably downfield chemical shifts and one (L^{26}) with upfield chemical shifts. L^{21}, Q^{24}, and L^{26} Hα CSs are perturbed by the ring current effect of the neighboring W^{25} aromatic residue because the two former protons lie in the plane of the indole ring while L^{26} Hα lies right above it. On the contrary, for spatial reasons E^{17} Hα must be unaffected by the W^{25} ring current because the distance between E^{17} Hα and the closest indole carbon (W^{25} Cγ) is ∼13 Å; therefore, the close to zero CSD indicates that the continuous α-helix has a kink point at this residue.

Division of the central α-helix into two helical subsets is in excellent agreement with the GLP-1 structure[17] where the N-terminal random coil segment (residues H^7−S^{14}) is followed by two helical segments (N-helix of S^{14}−E^{21} and C-helix of A^{25}−G^{36}) that are connected by a linker region (G^{22}−A^{24}). This linker provides flexibility for the long α-helix to access the nGLP-1R binding site.[14] Therefore, in Ex4 and E19, E^{17} has a role similar to that of the linker region in the GLP-1(7−37) α-helix.[17] Here, the N-helix spans residues D^9−E^{16}, while the C-helix spans A^{18}−E^{28}. Residues in the C-helix show much larger Hα chemical shift deviations than the residues in the N-helix (Figure 3). Via inspection of the structure of E19 (Figure 4m), it is evident that

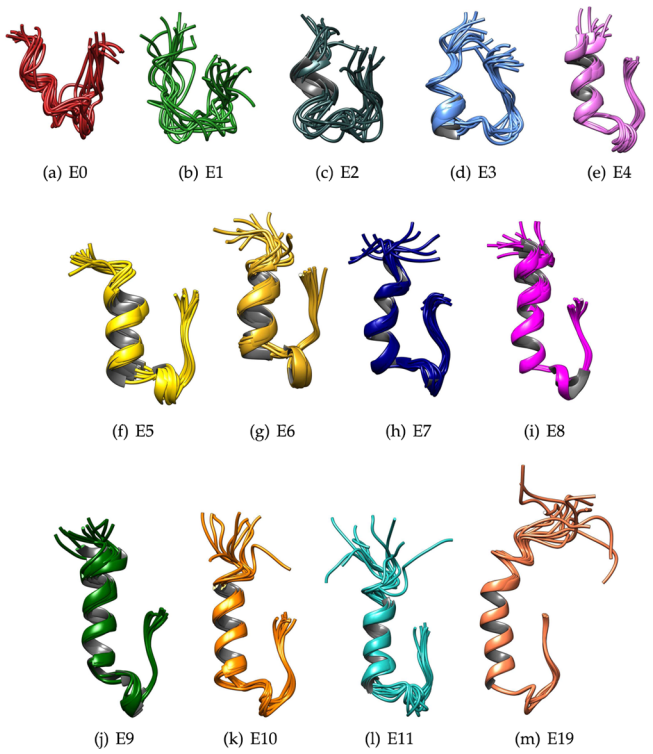

Figure 4. Ribbon representations of the NMR structural ensembles of the N-terminally elongated Trp cage variants.

as the C-terminal PPII helix folds back to W^{25} it interacts with the C-helix (several NOEs connect the two regions), while it has a minor direct effect on the N-helix (no NOEs are found between the C-terminal segment and the N-helix). The C-helix and the PPII helix together form the TC motif (A^{18}−S^{39}), and thus, the TC motif serves as an ideal C-cap for the helical core.

The helix inducing ability of the TFE/water mixed solvent was studied by comparing the Hα CSDs of E19 measured in H_2O and in 30% TFE and that of Ex4 measured in 30% TFE (Figure S3 of the Supporting Information). There is less difference between the spectra of $E19^{(30\%TFE)}$ and $Ex4^{(30\%TFE)}$ than between $E19^{(H_2O)}$

dx.doi.org/10.1021/bi500033c | *Biochemistry* 2014, 53, 3540−3552

Table 1. Folded Fractions of the N-Terminally Elongated Trp Cage Variants

name	sequence	T (°C)	folded fraction			
			CSD_{cage}	CSD_{helix}	$\chi_{F(cage)}$	$\chi_{F(helix)}$
Ex4 (30% TFE)	HGEGTFTSDLSKQMEEEAVRLFIEWLKNGGPSSGAPPPS	27	8.46	1.63	0.74	0.77
E19 (30% TFE)	HGEGTFTSDLSKQMEEEAVRLYIQWLKEGGPSSGRPPPS	27	10.25	1.77	0.89	0.87
E19	HGEGTFTSDLSKQMEEEAVRLYIQWLKEGGPSSGRPPPS	27	10.09	1.80	0.88	0.89
E11	DLSKQMEEEAVRLYIQWLKEGGPSSGRPPPS	27	9.99	1.80	0.87	0.89
E11	DLSKQMEEEAVRLYIQWLKEGGPSSGRPPPS	5	10.56	1.85	0.92	0.92
E10	LSKQMEEEAVRLYIQWLKEGGPSSGRPPPS	5	11.10	1.96	0.97	1.00
E9	SKQMEEEAVRLYIQWLKEGGPSSGRPPPS	5	10.80	1.78	0.94	0.88
E8	KQMEEEAVRLYIQWLKEGGPSSGRPPPS	5	10.84	1.80	0.94	0.89
E7	QMEEEAVRLYIQWLKEGGPSSGRPPPS	5	10.83	1.80	0.94	0.89
E6	MEEEAVRLYIQWLKEGGPSSGRPPPS	5	10.79	1.75	0.94	0.86
E5	EEEAVRLYIQWLKEGGPSSGRPPPS	5	10.57	1.72	0.92	0.83
E4	EEAVRLYIQWLKEGGPSSGRPPPS	5	9.60	1.74	0.84	0.85
E3	EAVRLYIQWLKEGGPSSGRPPPS	5	7.31	1.31	0.64	0.55
E2	AVRLYIQWLKEGGPSSGRPPPS	5	3.69	1.08	0.39	0.40
E1	VRLYIQWLKEGGPSSGRPPPS	5	1.10	1.00	0.30	0.35
E0	RLYIQWLKEGGPSSGRPPPS	5	1.79	0.94	0.25	0.30
TC	NLYIQWLKEGGPSSGRPPPS	5	9.89	1.63	0.86	0.78
TC	NLYIQWLKEGGPSSGRPPPS	27	3.88	1.25	0.54	0.51
folded reference	EEECVRLYIQWLKDGGPSSGRPPPC	15	11.49	1.96	1.00	1.00
unfolded reference	NLYIQWLKDGGPSSGRPPPpS	15	0.5	0.57	0.05	0.05

and $E19^{(30\%TFE)}$, implying that the four mutations that distinguish E19 from Ex4 have a weaker effect on the overall structure than the solvent composition does. Remarkably, the Hα CSD pattern of the C-helix of E19 is slightly perturbed; the Hα CSDs of Y^{22}, I^{23}, W^{25}, and L^{26} are reduced by ∼0.1 ppm, while that of K^{27} is increased by ∼0.05 ppm as the TFE is added to the solution. Also, a change can be observed in the helicity of the N-helix, where S^{11}, M^{14}, E^{15}, and E^{16} become more helical (Hα CSD reduced by ∼0.08 ppm). These effects are ascribed to the ability of TFE to stabilize helical conformations in peptides while disrupting the hydrophobic interactions of native proteins.[51]

Following Barua et al., we use CSD_{cage} and CSD_{helix} values to compare the relative stabilities of the different TC variants.[52] Table 1 and Table S1 of the Supporting Information list the calculated CSD values and the derived relative folded fractions χ_F.

On the basis of the CSD_{helix} and $\chi_{F(helix)}$ values, the most helical studied peptide is E10 with an apparent 100% helix population (same helicity as the folded reference construct). This seemingly contradicts the ECD data where E11 was the most helical peptide; however, the two methods measure the helicity in two different ways: ECD measures an ellipticity value to which the whole molecule contributes (n → π^* band of the amide bonds), while the CSD_{helix}-derived χ_F value reports on the helicity of the TC motif itself. In general, we conclude that the overall helicity of these peptides gradually increases from E0 to E11, while the further elongation (E11 → E19) does not further improve the helicity. In fact, E19 has a fold stability [$\chi_{F(cage)}$ and $\chi_{F(helix)}$] similar to that of E11, originating from the similar helical propensity as discussed above.

In E0, the N-terminal Asn → Arg substitution strongly destabilized the structure: $\chi_{F(cage)}$ and $\chi_{F(helix)}$ decreased from 86 to 25% and from 78 to 30%, respectively (Table 1). In the NMR spectra of E0, some slowly exchanging additional peaks appeared beside the main set of resonances (e.g., Y^{22} Hε#, W^{25} Hδ1, and W^{25} Hε1). The presence of peaks associated with the TC minor conformer was observed before under acidic conditions.[34,48] Many characteristic NOEs (Y^{22} Hδ#−P^{38} Hγ#; W^{25} Hδ1−R^{35} Hβ#,Hγ#; W^{25} Hη,Hζ2−P^{31} Hγ#; W^{25} Hε1−P^{36} Hα; etc.) indicate, however, that the folded 3D structure is still preserved in E0, but highly destabilized. The destabilization stems from the repulsion between the partial positive charge of the helix macrodipole at the N-terminus co-located with the positively charged Arg residue. On the other hand, the introduction of a negatively charged aspartate at the N-terminus of the Trp cage (e.g., as Asp^1 in Tc10b, DAYAQWLKDGGPSSGRPPPS) is highly favorable.[52] This is in line with the general observation that the helical content of model peptides (e.g., NH_2-XAKAA-AAKAAAAKAAGY-$CONH_2$) decreases as the N-terminal amino acid becomes more positive.[53]

The TC fold stability is restored during the gradual N-terminal elongation. Both the helix [$\chi_{F(helix)}$] and the cage [$\chi_{F(cage)}$] populations increase by ∼5−10% for each of the added residues, resulting in E1−E3 (Table 1). Although E3 is stabilized by the N-terminal negatively charged glutamate (Glu^{17}), it is still less stable than the shorter TC. However, the tendency is clear, and the stability is fully restored by the addition of the next glutamate (Glu^{16}) to the N-terminus, resulting in E4. In E4, Glu^{16} acts as an N-cap while Glu^{17} as a salt bridge-forming side chain interacting with Arg^{20}. $\chi_{F(cage)}$ increases further in E5 and reaches ∼90%. The next five constructs (E6−E10) have similar NMR spectral properties in terms of CSD and NOE patterns. The helix extension does not affect the folded population further: $\chi_{F(cage)}$ ranges between 92 and 97%. In E8, the positively charged N-terminal Lys^{12} does not destabilize the α-helix as Arg^{20} did in E0: it rather forms a salt bridge with either Glu^{15} or Glu^{16}, and the interaction shields the unfavorable positive charge at the terminus. Interestingly, E10 seems to be especially stable in comparison to E9 or E11; its helix population reaches the theoretical maximum [$\chi_{F(helix)} = 1$; i.e., E10 has the same helicity as the folded reference molecule], and the cage population is 97%. However, this exceptional stability was not apparent in the ECD measurements, as the latter method measures the content of the secondary structural elements (e.g., α-helix) rather than the fold compactness.

dx.doi.org/10.1021/bi500033c | Biochemistry 2014, 53, 3540−3552

Table 2. Numbers and Types of NOE Constraints and rmsds of the Structural Ensembles of the Reference TC as Well as Its 13 N-Terminally Elongated Analogues

	NOE constraints							rmsd[a]	
	i,i	*i,i* + 1	*i,i* + 2	*i,i* + 3	*i,i* + 4	*i,i* + *n*,*n* ≥ 5	∑	backbone	all atom
TC	170	106	25	31	18	67	415	0.05	1.78
E0	111	31	1	8	5	17	173	1.96	3.10
E1	126	3	0	3	2	12	146	2.37	3.63
E2	136	37	2	4	5	19	203	1.24	2.16
E3	140	65	7	14	9	30	265	1.90	1.03
E4	154	77	9	23	12	33	308	0.90	1.66
E5	176	100	17	29	15	41	378	0.58	2.21
E6	166	92	15	24	15	38	350	0.89	1.89
E7	187	88	10	35	16	37	373	0.82	2.42
E8	197	87	9	37	16	36	382	0.70	1.45
E9	203	106	20	48	32	61	470	0.69	1.49
E10	203	110	14	44	19	47	437	0.76	1.57
E11	174	61	3	46	21	53	358	1.37	2.28
E19	284	185	26	114	78	87	774	0.33[b]	1.15[b]

[a]Calculated using the Cα, CO, and N atoms, or all atoms of 3rd–S^{39}. [b]Calculated using the Cα, CO, and N atoms, or all atoms of D^{9}–S^{39}.

Via comparison of the folded fractions of Ex4$^{(30\%TFE)}$ and E19$^{(30\%TFE)}$, it becomes apparent that E19 has a stabilized fold with superior helicity and compactness [$\chi_{F(cage)}$ and $\chi_{F(helix)}$, as these values increase by ∼10% in E19$^{(30\%TFE)}$ with respect to those in Ex4$^{(30\%TFE)}$]: 0.74 < $\chi_{F(cage)}$ < 0.89, and 0.77 < $\chi_{F(cage)}$ < 0.87. Note that there is only minor difference in the $\chi_{F(cage)}$ and $\chi_{F(helix)}$ values between the E19 spectra recorded in water and in a 30% TFE solution. This implies that the TFE induces TC formation only in those molecules in which the TC fold is less stable in aqueous solution (Ex4); on the other hand, it has no effect on variants in which the TC fold is already compact enough in water (E19).

These findings corroborate the results of the ECD measurements.

The Designed Variants Preserve the TC Structure. All N-terminally elongated variants have the same TC fold, differing only at the N-termini. The TC fold is characterized by a compact tertiary structure that consists of an N-terminal α-helix, followed by a 3_{10}-helix (Gly^{29}–Gly^{34}) and a short polyproline II helix (Arg^{35}–Ser^{39}), all organized around the central Trp^{25} residue. Here, we summarize the observed minor structural differences of E0–E11 while a more comprehensive analysis is given for E19. The structure refinement statistics and the number of constraints employed in the ensemble calculations are listed in Table 2.

E0–E4. As discussed earlier, the Asn^{20} → Arg^{20} mutation highly destabilizes the TC structure because of the repulsion between the positive charge of Arg^{20} and the partially positive charge of the α-helix macrodipole at the N-terminus. In accordance with such stability loss, the total number of assignable NOEs is lower than the number of TCs (Table 2). The lower number of NOEs results in poorly defined structural ensembles for E0–E3. A ribbon representation of 10 superimposed structures with rmsds of 1.96, 2.26, 1.23, and 1.90 Å for backbone atoms are shown in panels a–d of Figure 4, respectively. Although the variation of the structures is large, the TC fold is apparent, as a handful of α-helix- and Trp cage-defining NOEs are observed in the NOESY spectra, e.g., Y^{22} Hα–W^{25} Hβ1,Hβ2; W^{25} Hζ2,Hη2–P^{31} Hγ#; W^{25} Hδ1–R^{35} Hγ#; or W^{25} Hζ2–P^{37} Hδ1 side-chain protons.

The NOESY spectrum of E4 contained an adequate number of interresidual NOEs for deriving a structural ensemble with a low backbone rmsd (0.71 Å) (Figure 4e). Most of the characteristic long-range NOEs are observed. The N-terminal α-helix is one turn longer than that of TC, and a favorable Glu^{17}–Arg^{20} salt bridge can stabilize this extended α-helix.

E5–E11. All of these peptides show the same overall structure displaying the characteristic TC features (Figure 4f–l). The N-terminal α-helix gradually extends, while the TC motif remains quasi unchanged. The NOE patterns are consistent with a continuous α-helix: many of the expected Hα^{i}–Hβ^{i+3} and Hα^{i}–Hβ^{i+4} NOEs are seen spanning the α-helix from the second N-terminal residue to Glu^{28}. The kink at Glu^{17} found by the CSD analysis is not apparent from the structures; several NOEs connect the C-terminal segment of the α-helix (C-helix) with the N-terminal part of it (N-helix). Interestingly, the aromatic side-chain resonances of Tyr^{22} in E10 were broadened, indicating that the rotation about the Cβ–Cγ axis slowed to the microsecond to millisecond time scale, while for all other peptides, this rotation was fast enough to give rise to single, degenerate Tyr^{22} Hδ# and Hε# resonances.

E19. The sequences of E19 and Ex4 differ at four positions only; namely, Y^{22}, Q^{24}, E^{28}, and R^{35} replace F^{22}, E^{24}, N^{28}, and A^{35}, respectively, of Ex4. All other residues are the same. In the PDB, both NMR and X-ray structures are available for Ex4; the NMR structure (PDB entry 1JRJ) was determined in a 30% TFE solution,[8] while a truncated Ex4 [Ex4(9–39), PDB entry 3C5T] was crystallized together with the N-terminal domain of the GLP-1R.[9]

In our study, the NMR structure of E19 was determined using 774 NOE constraints (PDB entry 2MJ9); 114 + 78 define the α-helix (*i,i* + 3 and *i,i* + 4 NOEs), and 87 define the overall structure (*i,i* + *n*,*n* > 4). However, no interresidual NOE was observed for residues of the N-terminal tail (H^{1}–T^{7}), fully supporting the idea that this segment is highly dynamic. Because of the high NOE density, the calculated structural ensemble is of good quality, represented by a small rmsd; the pairwise rmsd for residues 9–39 was 0.33 Å for the backbone atoms and 1.15 Å for all heavy atoms (Table 2).

The presence of exchange cross-peaks of the amide protons of residues 3–16 with water in the NOESY spectrum suggests that in time average these amides are partially or completely solvent exposed, which agrees well with the CSD data suggesting that the N-terminal segment (H^{1}–T^{7}) is disordered and the N-helix (D^{9}–E^{16}) is less stable than the C-helix (A^{18}–E^{28}). These data

dx.doi.org/10.1021/bi500033c | *Biochemistry* 2014, 53, 3540–3552

are well-reflected in the 10 conformers representing the 3D structure of E19 (Figure 4m). Continuous $CO^{i} \rightarrow NH^{i+4}$ hydrogen bonds are observed for residues M^{14}–E^{28}, while no single secondary structure is observed for the N-terminal tail (H^{1}–T^{7}). As found in the TC motif, residues G^{30}–G^{34} prefer to be a 3_{10}-helix rather than an α-helix conformer supported by the presence of $H\alpha^{i}$–HN^{i+2} NOEs and the absence of $H\alpha^{i}$–$H\beta^{i+3}$ NOEs. Of special interest are the salt bridges connecting residues D^{9}, K^{12}, E^{16}, and R^{20}; the side chain of K^{12} and E^{16} can alternate to interact with the oppositely charged residues downstream or upstream on the α-helix face, thereby largely stabilizing the overall helical fold.

The superpositions of the backbone atoms of the NMR structure of E19 with the NMR and X-ray structures of Ex4 are shown in panels a and b of Figure 5. Although the overall

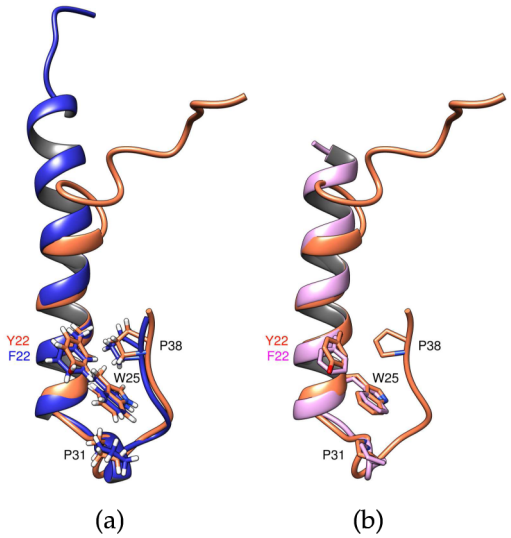

Figure 5. Ribbon representation of E19 [PDB entry 2MJ9 (coral)] with (a) the Ex4 NMR structure [PDB entry 1JRJ (blue)] and (b) the Ex4 X-ray structure [PDB entry 3C5T (orchid)]. Y^{22}/F^{22}, W^{25}, P^{31}, and P^{38} are displayed in all-atom representation. For the sake of clarity and a better comparison in panel b, the H atoms have been omitted from the E19 NMR structure.

structures of these compared molecules are similar [backbone rmsds of residues 15–39 between E19 and $Ex4^{(NMR)}$ and between E19 and $Ex4^{(X\text{-}ray)}$ of 0.74 and 0.81 Å, respectively], some differences also emerge. The major distinction between the NMR structure of E19 and Ex4 is the apparent mobility and orientation of residues 5–14; $Ex4^{(30\%TFE)}$ seems to be more rigid and helical here than $E19^{(H_2O)}$. The helix of E19 is less defined because of the minimal helix-positioning NOEs between T^{5} and M^{14}. The α-helix stretches between T^{5} and N^{28} in Ex4 and between D^{9} and E^{28} in E19. In both peptides, the N-terminal tail is disordered, which is a prerequisite for bioactivity.[50]

The differences between the $E19^{(NMR)}$ and $Ex4^{(X\text{-}ray)}$ structures become apparent when the side-chain orientations of some helix-forming residues are analyzed, particularly those of D^{9}, K^{12}, E^{17}, and R^{20}. In the $Ex4^{(X\text{-}ray)}$ structure, D^{9} is the first N-terminal residue with a high *B* factor showing no polar contact with the surrounding side chains. In E19 [and in $Ex4^{(NMR)}$], D^{9} forms a helix-stabilizing salt bridge with K^{12}. Similarly, E^{17} has no direct intermolecular interaction in $Ex4^{(X\text{-}ray)}$, while it forms a salt bridge with R^{20} in the $E19^{(NMR)}$ structure. On the other hand, in $Ex4^{(X\text{-}ray)}$, the side chain of R^{20} interacts with the side chain of E^{128} of nGLP-1R.

Fold Fluctuation Determined by NMR Backbone Dynamics. Local backbone dynamics of TC, E5, E11, and E19 samples were investigated using ^{15}N longitudinal (R_1) and transverse (R_2) relaxation rates and steady-state heteronuclear NOEs (Figure S8 of the Supporting Information) at 27 °C. These relaxation parameters were analyzed with the reduced spectral density mapping (RSDM) approach[40,43–45] (Figure 6). The more widespread Lipari–Szabo model-free analysis[54,55] was not applied because its assumptions do not hold for this system, particularly at marginal structural stability (e.g., TC at 27 °C), and the time scales of internal and overall motion are not independent; moreover, if dimerization or oligomerization occurs, then a single τ_c rotational correlation time or rotational diffusion tensor cannot describe the overall motion. The RSDM approach does not use any assumption regarding the time scale of motions or the shape and size of the molecule; therefore, it can confidently be applied to characterize even highly flexible polypeptides.

As the length of the N-terminal α-helix increases so does the average $J(0)$ value. This phenomenon is a result of the altered form of the rotational diffusion tensor. Starting from a globular TC fold, the molecule adopts the shape of a prolate rotor; then, it forms higher-molecular weight oligomers (*vide infra*). Besides, an elevated $J(0)$ indicates sites with slow time scale backbone motion (R_{ex}). Some residues (e.g., E^{15}, G^{30}, and S^{32} in E11 or E^{16}, Y^{22}, and K^{27} in E19) show exceptionally increased $J(0)$ values that could refer to microsecond to millisecond dynamic processes at those sites (Figure 6).

The $J(\omega_N)$ value does not seem to change substantially with the overall shape of the molecule (i.e., the length of the α-helix). Therefore, very similar $J(\omega_N)$ values were measured for E5, E11, and E19, especially in the core α-helical region (Y^{22}–G^{30}). The apparent decrease in the $J(\omega_N)$ of TC with respect to E5, E11, and E19 reflects the fact that at 27 °C the folded fraction of TC is only ~54% while that of E11 and E19 is ~90% (see Table 1). Interestingly, for the residues in the 3_{10}-helix, the $J(\omega_N)$ values increase with the length of the molecules (TC → E5 → E11 → E19), which indicates that motions around 50 MHz become more prevalent here.

The sequence dependence of the $J(0.87\omega_H)$ values corroborates the observations made for $J(\omega_N)$ described above. TC is the most flexible molecule among the studied elongated variants; thus, it has the highest average $J(0.87\omega_H)$. As the length of the α-helix increases, the stability of the molecules increases and their $J(0.87\omega_H)$ value decrease. Apart from the N-terminal tail of E19, the amides of S^{34} and G^{35} are the most flexible in all constructs, usually more flexible than the C-terminal S^{39}.

The potential R_{ex} contributions of E19 relaxation was examined by combining the $J(0)$ values measured independently at two spectrometer frequencies (500 and 700 MHz), and the proportionality factor (ϕ, $R_{ex} = \phi\omega_N^2$) was derived using published methods.[56] A plot of the ϕ values versus the protein sequence (Figure 6d) indicates that there is a general increase in almost all $J(0)$ values with increasing field with typical values between 10×10^{-9} and 30×10^{-9} ns rad^{-1}. This reflects a widespread exchange process that affects the whole molecule such as a slow time scale dimerization or oligomerization. The highest ϕ values were observed for Y^{22}, K^{27}, and G^{30} in the range of $40–60 \times 10^{-9}$ ns rad^{-1}, which corresponds to R_{ex} contributions of 8.9 ± 6.8, 6.8 ± 4.2, and 10.8 ± 4.6 s^{-1}, respectively. The slow exchange of K^{27} and G^{30} could be in

dx.doi.org/10.1021/bi500033c | *Biochemistry* 2014, 53, 3540–3552

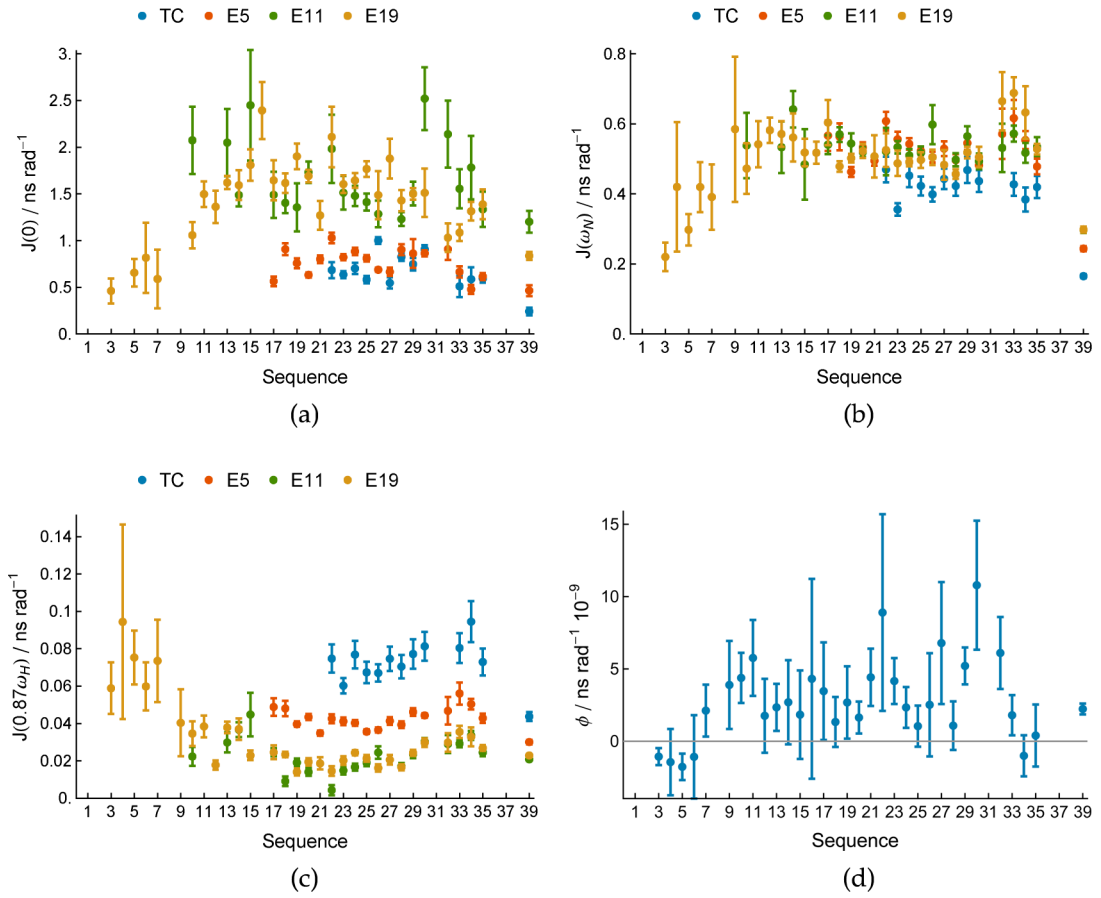

Figure 6. (a) $J(0)$, (b) $J(\omega_N)$, and (c) $J(0.87\omega_H)$ spectral density values of TC, E5, E11, and E19 measured at 27 °C at a B_0 field strength of 11.74 T. (d) Exchange parameter ϕ vs the primary sequence of E19.

Table 3. Diffusion Coefficients and Apparent Molecular Masses of E19 and Ex4 in 10% D_2O/90% H_2O and 30% TFE-d_2/70% H_2O Mixtures at 5, 16, and 27 °C

		10% D_2O/90% H_2O			30% TFE-d_2/70% H_2O		
	T (°C)	D_{obs} ($\times 10^{-11}$ m^2/s)	D_{st} ($\times 10^{-11}$ m^2/s)	M_w^{app} (kDa)	D_{obs} ($\times 10^{-11}$ m^2/s)	D_{st} ($\times 10^{-11}$ m^2/s)	M_w^{app} (kDa)
E19	5	7.44 ± 0.07	12.3 ± 0.12	8.5	3.55 ± 0.05	9.41 ± 0.08	19.0
	16	10.8 ± 0.5	13.3 ± 0.6	6.7	6.05 ± 0.01	11.96 ± 0.02	9.2
	27	16.2 ± 0.4	13.7 ± 0.3	6.1	9.84 ± 0.07	13.8 ± 0.1	6.0
Ex4	5	6.99 ± 0.02	11.56 ± 0.03	10.2	3.25 ± 0.06	8.61 ± 0.11	24.9
	16	10.22 ± 0.06	12.6 ± 0.08	7.9	5.91 ± 0.05	11.69 ± 0.06	9.9
	27	14.3 ± 0.3	12.6 ± 0.3	8.0	9.46 ± 0.06	13.27 ± 0.09	6.8

connection with the rearrangement of the 3_{10}-helix region, which is the initial step of TC unfolding.[34]

The backbone relaxation measurements confirmed the observations of the Hα chemical shift deviation analysis. We found a correlation between the magnitude of the Hα CSD and the rigidity of the backbone NH vector (compare Figures 3 and 6c and Figure S9f of the Supporting Information). Both of these methods identified the N-terminal tail (H^1–S^8) as a flexible, unstructured segment, the N-helix (D^9–E^{16}) as a moderately stable, structured segment with increased mobility, and the C-helix as rigid, stable, helical segment. The NOESY-based structure calculation does not pick up the interface between the N- and C-helix; however, as NOE-based calculations reflect the average structure, fast local confined backbone fluctuations are ignored. Thus, a combined study of chemical shifts, structure, and dynamics is needed to characterize the complex conformational dynamics of a protein. These studies can be complemented with temperature-dependent folding measurements, and hence, the energetic aspects of the protein's stability and flexibility can be evaluated.

Ex4 Forms Higher-Order Associates Than E19 Does. Previous studies reported that both GLP-1 and Ex4 show significant self-association *in vitro* at close to physiological pH and temperature, resulting in amyloid-like fibrils (GLP-1)[29,57] and broadened NMR signals (Ex4).[8,25,58] The self-association number of the 2 mM Ex4 sample at 298 K was approximated to be three (trimer) in water and between two (dimer) and three (trimer) in a 30% TFE/70% H_2O solution.[58]

To obtain the translational diffusion coefficients (D) and the apparent molecular mass (M_w^{app}) of Ex4 and E19, we performed pseudo two-dimensional DOSY experiments at three different temperatures (5, 16, and 27 °C) in an aqueous solution and in a 30% TFE/70% H_2O solution on 0.5 mM peptide samples. To take into account the differences in temperature and viscosity

dx.doi.org/10.1021/bi500033c | *Biochemistry* 2014, 53, 3540–3552

among different conditions, we converted the measured diffusion coefficients to standard conditions (20 °C, water).[39] The measured diffusion coefficients (D_{obs}), the calculated standard condition diffusion coefficients (D_{st}), and the apparent molecular masses of E19 and Ex4 are compared in Table 3. As monomers, Ex4 and E19 have molecular masses of 4.2 and 4.3 kDa, respectively; thus, the calculated 6−28 kDa M_w^{app} implies that both of these molecules exist in equilibrium between multiple states with different self-association numbers.

As listed in Table 3 (and shown in Figure S4 of the Supporting Information), E19 exhibits a somewhat larger diffusion coefficient and thus a lower apparent molecular mass than Ex4 under all six measured conditions. This difference is rather small, implying that only a small perturbation occurred in the intermolecular interactions that hold together the complexes. As expected, the self-association propensity decreases with an increase in temperature; in water at 5 °C, the majority of the molecules form dimers, and at 27 °C, the equilibrium is shifted toward the monomer. This is in line with the observed narrowing of the NMR signals at higher temperatures. The self-association is weak and transient and occurs relatively fast on the NMR time scale (intermediate exchange regime); therefore, the observed diffusion coefficient appears as the population-weighted average of the diffusion coefficients of the monomer, dimer, trimer, etc.

A uniform dimerization with a clear interaction surface was not captured during the NOE-based structure determination of E19. No intermolecular NOEs define the relative orientation of the two (or more) interacting molecules, which implies that no single structure can represent the dimer or oligomer states. Most likely, the long α-helix represents the interacting surface because the NH amide resonances of the residues in the α-helix showed relatively broader resonances than those in the N-terminal tail or at the 3_{10}-helix region did. The latter finding was also supported by backbone relaxation measurements; the transverse relaxation rate was significantly higher in this region than at the unstructured N-terminal tail or at the C-terminal region (*vide supra*). Previous medium dependence studies also established that the segment spanning Gln[13] and Leu[26] could be responsible for nonspecific helix bundle formation in water and organic solvents.[25]

A TFE/water mixed medium induces α-helix formation in polypeptides and thus facilitates the self-association of both Ex4 and E19. Most probably, the TFE cosolvent favors intermolecular helix−helix interaction over intramolecular Trp cage formation and therefore promotes oligomerization.[51] In 30% TFE at low temperatures, the equilibrium is shifted toward higher-order associate states (trimer ⇌ tetramer for E19 and pentamer ⇌ hexamer for Ex4) than in the absence of TFE (dimer ⇌ trimer for both E19 and Ex4), but the decrease in self-association number with temperature is more drastic in a 30% TFE solution than it is in water.

E19 and Ex4 Show Comparable Insulin Stimulating Activity. The secretory responses of INS-1E cells to various GLP-1R agonist stimuli were tested in the presence of 15 mM glucose, over a 30 min incubation period (see Figure 7). First, we conducted a pilot glucose-stimulated insulin secretion study to set the conditions for the GLP-1R agonist peptide testing. We stimulated the cells with 15 mM glucose alone and observed a maximal 2.35-fold increase in the level of insulin secretion compared to that with basal 2.5 mM glucose [on average, we saw a 1.79 ± 0.17-fold increase in response to 15 mM glucose (n = 7)]. Next, as a negative control, we tested the effect of GLP-1R agonist Ex4 at a low glucose concentration (2.5 mM) and could not see a substantially increased level of insulin secretion, as was expected (data not shown). In contrast, the level of insulin secretion was markedly increased when GLP-1R agonist Ex4 was added (20 nM) at a glucose concentration of 15 mM.

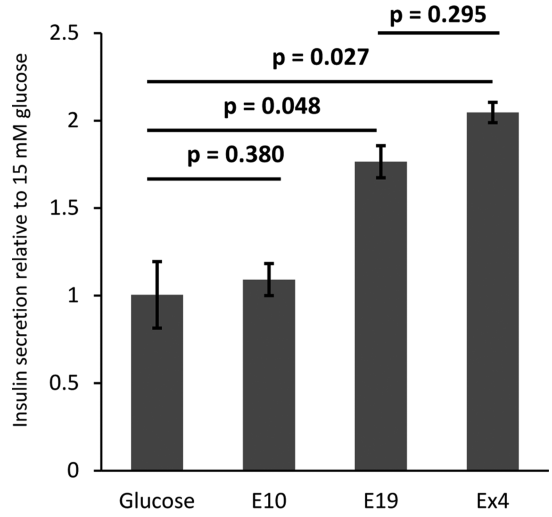

Figure 7. Relative change in insulin secretion in the presence of 15 mM glucose and 20 nM E10, E19, and Ex4 compared to the response to 15 mM glucose alone in INS-1E cells. Values are presented as means ± the standard error of the mean.

Compared with the level of insulin release at 15 mM glucose, there was a 2.05 ± 0.06-fold increase in the level of insulin secretion in response to 20 nM Ex4 [mean ± standard error of the mean (n = 9)]. As displayed in Figure 7, the insulin secreting ability of E19 is comparable to that of Ex4; however, it is slightly reduced relative to that of Ex4 by 15 ± 5% [statistically insignificant (n = 6)]. The truncation of the first nine residues of E19 converted peptide E10 to a weak antagonist or to a nonbinding peptide as its insulin secretion ability is comparable to that of glucose alone (p = 0.380; n = 5). However, further study is needed to test the nGLP-1R binding ability of E10. Previous studies established that Ex4(9−39) and other truncated variants of Ex4 bind the nGLP-1R with high affinity and thus act as strong antagonists in competitive binding studies;[3,9] therefore, it is likely that E10 binds the nGLP-1R and acts as an antagonist.

It is noteworthy that the level of insulin secretion in our cultured INS-1E cell line around passage 100−120 is considerably lower than what was reported previously.[46] Therefore, the results should be interpreted within the context of this particular experiment.

■ DISCUSSION

Much effort has been spent to improve the *in vivo* half-life, binding affinity, and activity of the therapeutic antidiabetic drug Exendin-4 (Ex4) by chemical modification, either within the sequence, e.g., replacing α-amino acids with β-amino acids,[58] or by side-chain conjugation, e.g., with fatty acids[59] or hylauronate.[60] In this study, our goal was to stabilize its structure, improve its water solubility, and weaken its self-association ability to facilitate future drug formulation.

Because the helicity of the peptides often correlates with their affinity and bioactivity, several studies attempted to stabilize the α-helix of different class B GPCR ligands. For instance, intramolecular lactam bridges or D-amino acids were introduced into the sequence of GLP-1[61,62] and CRF[21,63] to increase the ligands' α-helical propensity and to elucidate the optimal

dx.doi.org/10.1021/bi500033c | *Biochemistry* 2014, 53, 3540−3552

receptor-bound conformations. Constrained α-helix-favoring linkers (AAAA or EKEK) were incorporated into the sequence of GIP, resulting in highly potent GIP receptor antagonists.[64]

Our method for the stabilization of the α-helical conformation of Ex4 is a mild mutational approach in which the structurally optimized Trp cage (TC) miniprotein[32,33] serves as an ideal C-cap. It has been demonstrated that the TC motif can be used to stabilize moderately structured α-helices when it is introduced at the C-terminus.[24] Here we systematically increased the length of the TC motif with the corresponding amino acid residues of Ex4 and analyzed the structural consequences (stability, dynamics, and aggregation) of such an elongation by ECD and NMR spectroscopy.

First, we replaced the N-terminal Asn^{20} of TC with the corresponding Arg^{20} residue of Ex4 because this latter side chain is crucial for receptor binding.[10] We found that this modification destabilized the fold because of the repulsion between the positively charged N-terminal Arg and the positively charged helix macrodipole. With further N-terminal elongation, the helicity gradually increased and the peptides' structures were further stabilized. The 39-residue E19 is 20−30% more helical than Ex4 in both aqueous and helix-inducing media (30% TFE). The solution structures of Ex4 and E19 are rather similar: they include an N-terminal, highly flexible tail (His^1−Ser^8), an α-helix spanning Asp^9−Lys^{27}, and a well-formed C-terminal Trp cage motif in the segment of Ala^{18}−Ser^{39}. The only noteworthy difference appears at the N-terminal tail: in the 30% TFE solution, the α-helix of Ex4 begins one turn earlier than that of E19 in water.

The nine C-terminal residues of Ex4 have very weak electron density in the nGLP-1R-bound X-ray structure (PDB entry 3C5T), which suggests that this segment might be in an undocked, highly fluxional state, and the presence of Trp cage is not necessary for the optimal receptor−ligand interaction.[9] On the other hand, fluorescence studies of free and receptor-bound Ex4 implied that the Trp cage motif can be present at least partially in the nGLP-1R-bound state.[23] These concerns raise the question of whether it is necessary to have a ligand with a flexible C-terminal tail (as in Ex4) or no tail at all (as in GLP-1) or whether the flexibility of the C-terminal segment affects the binding affinity. Because Ex4 and E19 show comparable insulin secreting ability, we speculate that the nine C-terminal residues only help the preformation of the α-helix and have no role in the receptor−ligand interaction.

Previous studies established that structurally destabilized TC variants (e.g., serine-phosphorylated variants) easily polymerize into amyloid fibrils when highly concentrated samples are incubated at 37 °C.[65] Similarly, at higher concentrations (1−30 mM), E0, E5, and E10 analogues display an irreversible α-helix → β-sheet folding transition,[66] indicating that self-association is a general process among Trp cage and related polypeptides. For Ex4, the extreme, residue specific line broadening observed in the NMR spectra and the concentration-dependent change in its far-UV ECD spectra are also clear indications of oligomer formation.[25,58] With diffusion measurements, here we quantitatively analyzed the self-association ability of Ex4 and E19 in an aqueous medium as well as in a 30% TFE solution. We found that the observed level of oligomerization was always higher for Ex4 than for E19; that is, E19 is less prone to self-association. This observation provides evidence of the role of the Trp cage motif in the prevention of helix−helix interaction: oligomerization is initiated when the increase in energy associated with Trp cage formation is smaller than the increase in energy upon burial of the hydrophobic surface of the amphipathic α-helix. Thus, an energetically more favorable Trp cage formation (as in E19) prevents self-association. Organic cosolvents (e.g., TFE) favor α-helix over Trp cage formation and thus shift the equilibrium toward multimerization, and this explains the higher association number observed in the aqueous TFE solution.

In summary, we propose here that the rational design of the TC head of Ex4 stabilizes the central α-helical segments, increases 3D fold stability and water solubility, and, thus, opens new routes of creating new antidiabetics with lower aggregation propensities. The designed E19 molecule has the same tertiary structure in H_2O that Ex4 has in a 30% TFE solution; it is more helical than Ex4 under all studied conditions, and it is less prone to oligomerization and meanwhile has a well-preserved biological activity. These results suggest that other chemical or mutational modifications that facilitate the preformation of the α-helix but prevent significant self-association may result in more potent therapeutic drug candidates with improved pharmacokinetic properties.

■ ASSOCIATED CONTENT

Supporting Information

Results of near-UV measurements, details of the chemical shift deviation calculation, a plot of Hα chemical shift deviations of E11, E9, E7, E5, E3, and E1, and Ex4 and E19 in 30% TFE, a plot of the DOSY intensity decay of E19 and Ex4, NOE charts for E0−E11, R_1, R_2, and ^1H−^{15}N NOE data of TC, E5, E11, and E19, and $J(0)$, $J(\omega_N)$, and $J(0.87\omega_H)$ values of E19 measured at a spectrometer frequency of 700 MHz. This material is available free of charge via the Internet at http://pubs.acs.org.

■ AUTHOR INFORMATION

Corresponding Author

*E-mail: perczel@chem.elte.hu. Phone: +36 1 372-2500/1653. Fax: +36 1 372-2620.

Funding

This work was supported by grants from the Hungarian Scientific Research Fund (Grants OTKA NK101072, TAMOP-4.2.2.A-11/1/KONV-2012-0047, and TÁMOP-4.2.1-B-09/1/KMR-2010-0003).

Notes

The authors declare no competing financial interest.

■ ACKNOWLEDGMENTS

We thank Zoltán András Tuza for the preparation of the NOE charts. The INS-1E cell line was a kind gift of Prof. Claes Wollheim and Prof. Pierre Maechler, University of Geneva.

■ ABBREVIATIONS

ECD, electronic circular dichroism; Ex4, Exendin-4; GLP-1, glucagon-like peptide-1; GPCR, G-protein-coupled receptor; nGLP-1R, N-terminal domain of the glucagon-like peptide-1 receptor; KRBH, Krebs-Ringer bicarbonate HEPES buffer; NMR, nuclear magnetic resonance; rmsd, root-mean-square deviation; RSDM, reduced spectral density mapping; SPPS, solid-phase peptide synthesis; TC, Trp cage; TFE, trifluoroethanol.

■ ADDITIONAL NOTE

[a]The Asp^{28}−Arg^{35} salt bridge could be another option with an even higher stabilizing power.[47]

REFERENCES

(1) Eng, J., Kleinman, W. A., Singh, L., Singh, G., and Raufman, J. R. (1992) Isolation and characterization of exendin-4, an exendin-3 analogue, from *Heloderma suspectum* venom. Further evidence for an exendin receptor on dispersed acini from guinea pig pancreas. *J. Biol. Chem. 267*, 7402−7405.

(2) Göke, R., Fehmann, H. C., Linn, T., Schmidt, H., Krause, M., Eng, J., and Göke, B. (1993) Exendin-4 is a high potency agonist and truncated exendin-(9−39)-amide an antagonist at the glucagon-like peptide l-(7−36)-amide receptor of insulin-secreting β-cells. *J. Biol. Chem. 268*, 19650−19655.

(3) Montrose-Rafizadeh, C., Yang, H., Rodgers, B. D., Beday, A., Pritchette, L. A., and Eng, J. (1997) High potency antagonists of the pancreatic glucagon-like peptide-1 receptor. *J. Biol. Chem. 272*, 21201−21206.

(4) Young, A. A., Gedulin, B. R., Bhavsar, S., Bodkin, N., Jodka, C., Hansen, B., and Denaro, M. (1999) Glucose-lowering and insulin-sensitizing actions of exendin-4: Studies in obese diabetic (ob/ob, db/db) mice, diabetic fatty Zucker rats, and diabetic rhesus monkeys (*Macaca mulatta*). *Diabetes 48*, 1026−1034.

(5) Gallwitz, B., Ropeter, T., Morys-Wortmann, C., Mentlein, R., Siegel, E. G., and Schmidt, W. E. (2000) GLP-l-analogues resistant to degradation by dipeptidyl-peptidase IV in vitro. *Regul. Pept. 86*, 103−111.

(6) Green, B. D., and Flatt, P. R. (2007) Incretin hormone mimetics and analogues in diabetes therapeutics. *Best Pract. Res., Clin. Endocrinol. Metab. 21*, 497−516.

(7) Bhavsar, S., Mudaliar, S., and Cherrington, A. (2013) Evolution of exenatide as a diabetes therapeutic. *Curr. Diabetes Rev. 9*, 161−193.

(8) Neidigh, J. W., Fesinmeyer, R. M., Prickett, K. S., and Andersen, N. H. (2001) Exendin-4 and glucagon-like-peptide-1: NMR structural comparisons in the solution and micelle-associated states. *Biochemistry 40*, 13188−13200.

(9) Runge, S., Thogersen, H., Madsen, K., Lau, J., and Rudolph, R. (2008) Crystal structure of the ligand-bound glucagon-like peptide-1 receptor extracellular domain. *J. Biol. Chem. 283*, 11340−11347.

(10) Adelhorst, K., Hedegaard, B. B., Knudsen, L. B., and Kirk, O. (1994) Structure-activity studies of glucagon-like peptide-1. *J. Biol. Chem. 269*, 6275−6278.

(11) Gallwitz, B., Witt, M., Paetzold, G., Morys-Wortmann, C., Zimmermann, B., Eckart, K., Fölsch, U. R., and Schmidt, W. E. (1994) Structure/activity characterization of glucagon-like peptide-1. *Eur. J. Biochem. 225*, 1151−1156.

(12) Doyle, M. E., Theodorakis, M. J., Holloway, H. W., Bernier, M., Greig, N. H., and Egan, J. M. (2003) The importance of the nine-amino acid C-terminal sequence of exendin-4 for binding to the GLP-1 receptor and for biological activity. *Regul. Pept. 114*, 153−158.

(13) Al-Sabah, S., and Donnelly, D. (2004) The primary ligand-binding interaction at the GLP-1 receptor is via the putative helix of the peptide agonists. *Protein Pept. Lett. 11*, 9−14.

(14) Underwood, C. R., Garibay, P., Knudsen, L. B., Hastrup, S., Peters, G. H., Rudolph, R., and Reedtz-Runge, S. (2010) Crystal structure of glucagon-like peptide-1 in complex with the extracellular domain of the glucagon-like peptide-1 receptor. *J. Biol. Chem. 285*, 723−730.

(15) Donnelly, D. (2012) The structure and function of the glucagon-like peptide-1 receptor and its ligands. *Br. J. Pharmacol. 166*, 27−41.

(16) Braun, W., Wider, G., Lee, K. H., and Wüthrich, K. (1983) Conformation of glucagon in a lipid-water interphase by ^{1}H nuclear magnetic resonance. *J. Mol. Biol. 169*, 921−948.

(17) Thornton, K., and Gorenstein, D. G. (1994) Structure of glucagon-like peptide (7−36) amide in a dodecylphosphocholine micelle as determined by 2D NMR. *Biochemistry 33*, 3532−3539.

(18) Venneti, K. C., and Hewage, C. M. (2011) Conformational and molecular interaction studies of glucagon-like peptide-2 with its N-terminal extracellular receptor domain. *FEBS Lett. 585*, 346−352.

(19) Alana, I., Parker, J. C., Gault, V. A., Flatt, P. R., O'Harte, F. P. M., Malthouse, J. P. G., and Hewage, C. M. (2006) NMR and alanine scan studies of glucose-dependent in-sulinotropic polypeptide in water. *Biol. Chem. 281*, 16370−16376.

(20) Sun, C., Song, D., Davis-Taber, R. A., Barrett, L. W., Scott, V. E., Richardson, P. L., Pereda-Lopez, A., Uchic, M. E., Solomon, L. R., Lake, M. R., Walter, K. A., Hajduk, P. J., and Olejniczak, E. T. (2007) Solution structure and mutational analysis of pituitary adenylate cyclase-activating polypeptide binding to the extracellular domain of PAC1-RS. *Proc. Natl. Acad. Sci. U.S.A. 104*, 7875−7880.

(21) Spyroulias, G. A., Papazacharias, S., Pairas, G., and Cordopatis, P. (2002) Monitoring the structural consequences of Phe12→D-Phe and Leu15→Aib substitution in human/rat corticotropin releasing hormone. Implications for design of CRH antagonists. *Eur. J. Biochem. 269*, 6009−6019.

(22) Thorens, B., Porret, A., Buhler, L., Deng, S. P., Morel, P., and Widmann, C. (1993) Cloning and functional expression of the human islet GLP-1 receptor. Demonstration that exendin-4 is an agonist and exendin-(9−39) an antagonist of the receptor. *Diabetes 42*, 1678−1682.

(23) Runge, S., Schimmer, S., Oschmann, J., Schiodt, C. B., Knudsen, S. M., Jeppesen, C. B., Madsen, K., Lau, J., Thogersen, H., and Rudolph, R. (2007) Differential structural properties of GLP-1 and exendin-4 determine their relative affinity for the GLP-1 receptor N-terminal extracellular domain. *Biochemistry 46*, 5830−5840.

(24) Lin, J. C., Barua, B., and Andersen, N. H. (2004) The helical alanine controversy: An (Ala)6 insertion dramatically increases helicity. *J. Am. Chem. Soc. 126*, 13679−13684.

(25) Hudson, F. M., and Andersen, N. H. (2004) Exenatide: NMR/CD evaluation of the medium dependence of conformation and aggregation state. *Biopolymers 76*, 298−308.

(26) Schubert, D., Behl, C., Lesley, R., Brack, A., Dargusch, R., Sagara, Y., and Kimura, H. (1995) Amyloid peptides are toxic via a common oxidative mechanism. *Proc. Natl. Acad. Sci. U.S.A. 92*, 1989−1993.

(27) Fowler, S. B., Poon, S., Muff, R., Chiti, F., Dobson, C. M., and Zurdo, J. (2005) Rational design of aggregation-resistant bioactive peptides: Reengineering human calcitonin. *Proc. Natl. Acad. Sci. U.S.A. 102*, 10105−10110.

(28) Onoue, S., Ohshima, K., Debari, K., Koh, K., Shioda, S., Iwasa, S., Kashimoto, K., and Yajima, T. (2004) Mishandling of the therapeutic peptide glucagon generates cytotoxic amyloidogenic fibrils. *Pharm. Res. 21*, 1274−1283.

(29) Poon, S., Birkett, N. R., Fowler, S. B., Luisi, B. E., Dobson, C. M., and Zurdo, J. (2009) Amyloidogenicity and aggregate cytotoxicity of human glucagon-like peptide-1 (hGLP-1). *Protein Pept. Lett. 16*, 1548−1556.

(30) Perczel, A., Hudáky, P., and Pálfi, V. K. (2007) Dead-end street of protein folding: Thermodynamic rationale of amyloid fibril formation. *J. Am. Chem. Soc. 129*, 14959−14965.

(31) Rosenberg, A. S. (2006) Effects of protein aggregates: An immunologic perspective. *AAPS J. 8*, E501−E507.

(32) Neidigh, J. W., Fesinmeyer, R. M., and Andersen, N. H. (2002) Designing a 20-residue protein. *Nat. Struct. Biol. 9*, 425−430.

(33) Hudáky, P., Stráner, P., Farkas, V., Váradi, G., Táth, G., and Perczel, A. (2008) Cooperation between a salt bridge and the hydrophobic core triggers fold stabilization in a Trp-cage miniprotein. *Biochemistry 47*, 1007−1016.

(34) Rovó, P., Stráner, P., Láng, A., Bartha, I., Huszár, K., Nyitray, L., and Perczel, A. (2013) Structural insights into the Trp-cage folding intermediate formation. *Chem.—Eur. J. 19*, 2628−2640.

(35) Goddard, T., and Kneller, D. G. (1999) *SPARKY 3*, University of California, San Francisco.

(36) Bundi, A., and Wuthrich, K. (1979) ^{1}H-NMR Parameters of the Common Amino Acid Residues Measured in Aqueous Solutions of the Linear Tetrapeptides H-Gly-Gly-X-L-Ala-OH. *Biopolymers 18*, 285−297.

(37) Brünger, A. T., Adams, P. D., Clore, G. M., DeLano, W. L., Gros, P., Grosse-Kunstleve, R. W., Jiang, J. S., Kuszewski, J., Nilges, M., Pannu, N. S., Read, R. J., Rice, L. M., Simonson, T., and Warren, G. L. (1998) Crystallography & NMR system: A new software suite for macromolecular structure determination. *Acta Crystallogr. D54*, 905−921.

(38) Pettersen, E. E., Goddard, T. D., Huang, C. C., Couch, G. S., Greenblatt, D. M., Meng, E. C., and Ferrin, T. E. (2004) UCSF Chimera:

A visualization system for exploratory research and analysis. *J. Comput. Chem. 25*, 1605−1612.
(39) Yao, S., Howlett, G. J., and Norton, R. S. (2000) Peptide self-association in aqueous trifluoroethanol monitored by pulsed field gradient NMR diffusion measurements. *J. Biomol. NMR 16*, 109−119.
(40) Farrow, N. A., Zhang, O., Forman-Kay, J. D., and Kay, L. E. (1995) Comparison of the Backbone Dynamics of a Folded and an Unfolded SH3 Domain Existing in Equilibrium in Aqueous Buffer. *Biochemistry 34*, 868−878.
(41) Farrow, N. A., Zhang, O., Forman-Kay, J. D., and Kay, L. E. (1994) A heteronuclear correlation experiment for simultaneous determination of ^{15}N longitudinal decay and chemical exchange rates of systems in slow equilibrium. *J. Biomol. NMR 4*, 727−734.
(42) Farrow, N. A., Zhang, O., Szabo, A., Torchia, D. A., and Kay, L. E. (1995) Spectral density function mapping using ^{15}N relaxation data exclusively. *J. Biomol. NMR 6*, 153−162.
(43) Peng, J. W., and Wagner, G. (1992) Mapping of spectral density functions using heteronuclear NMR relaxation measurements. *J. Magn. Reson. 98*, 308−332.
(44) Peng, J. W., and Wagner, G. (1992) Mapping of the spectral densities of N-H bond motions in eglin c using heteronuclear relaxation experiments. *Biochemistry 31*, 8571−8586.
(45) Ishima, R., and Nagayama, K. (1995) Quasi-Spectral-Density Function Analysis for Nitrogen-15 Nuclei in Proteins. *J. Magn. Reson., Ser. B 108*, 73−76.
(46) Merglen, A., Theander, S., Rubi, B., Chaffard, G., Wollheim, C. B., and Maechler, P. (2004) Glucose sensitivity and metabolism-secretion coupling studied during two-year continuous culture in INS-IE insulinoma cells. *Endocrinology 145*, 667−678.
(47) Williams, D. V., Byrne, A., Stewart, J., and Andersen, N. H. (2011) Optimal salt bridge for Trp-cage stabilization. *Biochemistry 50*, 1143−1152.
(48) Rovó, P., Farkas, V., Hegyi, O., Szolomájer-Csikós, O., Tóth, G. K., and Perczel, A. (2011) Cooperativity network of Trp-cage miniproteins: Probing salt-bridges. *J. Pept. Sci. 17*, 610−619.
(49) Kieffer, T. J., and Habener, J. F. (1999) The glucagon-like peptides. *Endocr. Rev. 20*, 876−913.
(50) Siu, F. Y., et al. (2013) Structure of the human glucagon class B G-protein-coupled receptor. *Nature 499*, 444−449.
(51) Buck, M. (1998) Trifluoroethanol and colleagues: Cosolvents come of age. Recent studies with peptides and proteins. *Q. Rev. Biophys. 31*, 297−355.
(52) Barua, B., Lin, J. C., Williams, V. D., Kummler, R., Neidigh, J. W., and Andersen, N. H. (2008) The Trp-cage: Optimizing the stability of a globular miniprotein. *Protein Eng., Des. Sel. 21*, 171−185.
(53) Doig, A. J., and Baldwin, R. L. (1995) N- and C-capping preferences for all 20 amino acids in α-helical peptides. *Protein Sci. 4*, 1325−1336.
(54) Lipari, G., and Szabo, A. (1982) Model-free approach to the interpretation of nuclear magnetic resonance relaxation in macromolecules. 1. Theory and range of validity. *J. Am. Chem. Soc. 104*, 4546−4559.
(55) Lipari, G., and Szabo, A. (1982) Model-free approach to the interpretation of nuclear magnetic resonance relaxation in macromolecules. 2. Analysis of experimental results. *J. Am. Chem. Soc. 104*, 4559−4570.
(56) Peng, J. W., and Wagner, G. (1995) Frequency spectrum of NH bonds in eglin c from spectral density mapping at multiple fields. *Biochemistry 34*, 16733−16752.
(57) Jha, N. N., Anoop, A., Ranganathan, S., Mohite, G. M., Padinhateeri, R., and Maji, S. K. (2013) Characterization of amyloid formation by glucagon-like peptides: Role of basic residues in heparin-mediated aggregation. *Biochemistry 52*, 8800−8810.
(58) Wang, S., Yu, J., Li, W., and Li, F. (2011) Structural study of an active analog of EX-4 in solution and micelle associated states. *Biopolymers 96*, 348−357.
(59) Chae, S. Y., Choi, Y. G., Son, S., Jung, S. Y., Lee, D. S., and Lee, K. C. (2010) The fatty acid conjugated exendin-4 analogs for type 2 antidiabetic therapeutics. *J. Controlled Release 144*, 10−16.
(60) Kong, J.-H., Oh, E. J., Chae, S. Y., Lee, K. C., and Hahn, S. K. (2010) Long acting hyaluronate-exendin 4 conjugate for the treatment of type 2 diabetes. *Biomaterials 31*, 4121−4128.
(61) Murage, E. N., Schroeder, J. C., Beinborn, M., and Ahn, J. (2008) Search for α-helical propensity in the receptor-bound conformation of glucagon-like peptide-1. *Bioorg. Med. Chem. 16*, 10106−10112.
(62) Murage, E. N., Gao, G., Bisello, A., and Ahn, J. (2010) Development of potent glucagon-like peptide-1 agonists with high enzyme stability via introduction of multiple lactam bridges. *J. Med. Chem. 53*, 6412−6420.
(63) Gulyas, J., Rivier, C., Perrin, M., Koerber, S. C., Sutton, S., Corrigan, A., Lahrichi, S. L., Craig, A. G., Vale, W., and Rivier, J. (1995) Potent, structurally constrained agonists and competitive antagonists of corticotropin-releasing factor. *Proc. Natl. Acad. Sci. U.S.A. 92*, 10575−10579.
(64) Manhart, S., Hinke, S. A., Mcintosh, C. H. S., Pederson, R. A., and Demuth, H. (2003) Structure-function analysis of a series of novel GIP analogues containing different helical length linkers. *Biochemistry 42*, 3081−3088.
(65) Kardos, J., Kiss, B., Micsonai, A., Rovó, P., Kovács, J., Váradi, G., Tóth, G., and Perczel, A. Phosphorylation as Conformational Switch from the Native to Amyloid State: Trp-Cage as Protein Aggregation Model. (2014) submitted to *J. Phys. Chem B.*
(66) Farkas, V., Csordas, B., Hegyi, O., Toth, G. K., and Perczel, A. (2013) Foldamer Stability Coupled to Aggregation Propensity of Elongated Trp-Cage Miniproteins. *Eur. J. Org. Chem. 2013*, 3513−3522.